DESIGN AND EXPERIMENTAL STUDY OF A RESIDUAL FILM BALING DEVICE
/
残膜打包装置的设计与试验研究

Guan WANG[1)], Haolin WANG[2)], Zhihong TIAN[1)], Qi Wang[1)], Dong JI[1)], Fengbo LIU[1)*]
[1)] Liaoning Agricultural Vocational and Technical College, 76 Yucai Road, Yingkou 115009, China;
[2)] Design Department of Liaoning liaotuo Dayi Agricultural Machinery Co., Ltd, Fushun, 113000, China;
Tel: 18341895506; E-mail: j18341895506@126.com
Corresponding author: Fengbo LIU
DOI: https://doi.org/10.35633/inmateh-79-07

***Keywords:** residual film baling device; discrete element method (DEM); Rocky DEM; parameter optimization; response surface methodology (RSM).*

ABSTRACT
To address the problems of low bale-forming rate and loose compaction during the mechanized recovery of residual plastic film in farmland, a three-stage residual film baling device was developed. Based on the discrete element method (DEM), a flexible thin-shell model of the residual film was established, and dynamic simulation and parameter optimization of the baling process were carried out using Rocky DEM software. Combined with single-factor experiments and response surface methodology, the effects of baling chamber inclination angle, belt type, belt linear speed, and upper belt inclination angle on bale integrity and compaction were analyzed. The results showed that the bale-forming rate of the three-stage device reached 99.13%, and the bale density reached 83.75 kg/m³ under the optimal conditions: baling chamber inclination angle of 30°, upper belt inclination angle of 30°, belt linear speed of 2.3 m/s, and the use of a rough-surface belt. Field validation tests showed that the average density of the residual film bales was 91.4 kg/m³, with a prediction error of only 2.23 kg/m³ compared with the simulation results. The device operated stably and reliably. This study presents a high-efficiency residual film baling device with improved bale-forming rate and compaction performance through structural optimization and parameter tuning, providing technical support for efficient recovery and pollution control of residual plastic film in farmland.

摘要
针对机械化农田残膜回收过程中出现的袋装率低和薄膜包装松散的问题，本研究开发了一种三阶段残膜包装装置。基于离散元方法，建立了残膜的柔性薄壳模型，并使用 rockydem 完成了残膜包装过程的动态模拟和参数优化。结合单因素实验和响应面分析，探讨了包装腔角度、包装带类型、线速度和上带安装角度对包装完整性和紧凑性的影响规律。结果表明，三阶段装置的包装率达到了 99.13%，薄膜密度为 83.75 千克/立方米，当包装腔方位角为 30°、上带安装倾斜度为 30°、线速度为 2.3 米/秒且使用粗糙带时。现场验证显示，残膜袋的平均密度为91.4 千克/立方米，与模拟预测的误差仅为2.23 千克/立方米。该装置的运行稳定可靠。在本研究中，通过结构创新和参数优化，开发出了一种高回收率且结构紧凑的残膜包装装置，为农田残膜的高效回收和污染控制提供了技术支持。

INTRODUCTION
The extensive use of plastic films in agriculture has significantly enhanced crop productivity and efficiency in modern farming residual film. However, the improper disposal of agricultural plastic waste, particularly plastic films used for mulching, poses substantial environmental threats, contributing to soil pollution and microplastic contamination in agroecosystems (*Li et al., 2021; Zhang et al., 2020*). As the agricultural sector strives for sustainability, the development of effective residual film recovery technologies has become paramount (*Wang et al., 2021; Liu et al 2019*).

Recent advancements in machine design and technology have led to the emergence of residual film recovery machines, which facilitate the collection, recycling, and reprocessing of used plastic films (*Chen et al., 2020; Torres et al., 2022*). These machines not only streamline the waste recovery process but also significantly reduce labor costs and enhance recovery efficiency, thereby promoting sustainable agricultural practices (*Xu et al., 2023; Gao et al., 2022*).

Studies have demonstrated that implementing residual film recovery systems can result in considerable economic benefits for farmers (*Smith et al., 2019; Kim et al., 2021*). For instance, the recovery of used films allows for the recycling of valuable polymers back into the production cycle, reducing raw material dependency and lowering overall production costs (*Mao et al., 2022; Huang et al., 2020*). Moreover, these technologies contribute to closing the loop in agricultural plastics management, aligning with circular economy principles (*Anderson et al., 2021; Roberts et al., 2022*).

Despite significant strides in technology, challenges remain in achieving widespread adoption of residual film recovery machines (*Yuan et al., 2023; Deng et al., 2022*). Factors such as initial costs, maintenance, and the need for farmer education on proper usage significantly influence their implementation (*Liu et al., 2022; Choi et al., 2021*).

In conclusion, residual film recovery machines play a crucial role in mitigating the environmental impact of plastic films used in agriculture. Ongoing research and development efforts should focus on overcoming existing barriers, optimizing machine efficiency, and enhancing the circular economy in agriculture to ensure sustainable development. During the compression stage of the belt-type baling device, the residual film is still prone to probabilistic scattering and the movement trajectory is difficult to control, which is not conducive to the formation of high-density and stable formed residual film bales. Therefore, based on an in-depth analysis of the forming mechanism of the residual film in the baling chamber, structural constraints and parameter optimization are used to suppress the scattering and winding behaviors and improve the forming quality of the residual film package (*Xie et al., 2020; Tan et al., 2022*).

To address key problems such as the low bale-forming rate and loose baling during the mechanized recovery of residual plastic film in farmland, a three-stage belt-type residual film baling device was developed based on DEM and flexible thin-shell modeling technology *(Potyondy et al., 2004; Roessler et al., 2018)*. By establishing a dynamic model of residual film behavior in the baling chamber and performing three-dimensional simulations and parameter optimization using Rocky DEM software, the effects of key factors—including the inclination angle of the baling chamber, the type and linear speed of the baling belt, and the installation angle of the upper baling belt—on the integrity and compaction density of the residual film bales were systematically analyzed. The performance of the optimized parameter combination was further verified through field experiments.

MATERIALS AND METHODS

Overall structure and working principle

The residual film baling device mainly consists of a lower baling belt, a rear baling belt, and two side plates. Compared with conventional steel-roller-type baling systems, the belt-type baling structure reduces the overall machine weight and prevents film leakage between the rollers. Driven by the rear belt, the residual film rotates within the baling chamber and is gradually compacted to form a residual film bale. The overall structure of the device is shown in Fig. 1.

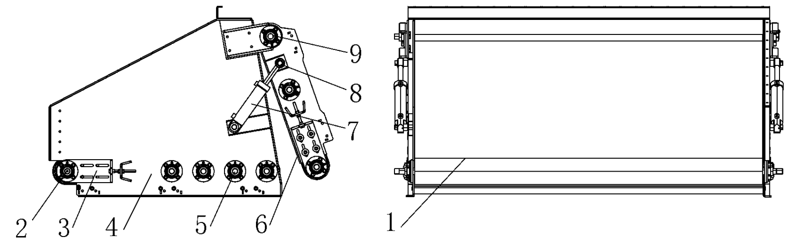

Fig. 1 - Basic structure of the residual film baling device

1. Discharge belt; 2. Lower belt drive roller; 3. Tension adjustment mechanism; 4. Side plates; 5. Support roller; 6. Rear baling belt; 7 Hydraulic cylinder; 8. Rear belt drive roller 9. Drive roller.

The lower baling belt is tensioned over the drive roller by means of a tension adjustment mechanism. The drive roller is fixed to the two side plates by bolted connections. For unloading, the rear baling mechanism can be lifted by a hydraulic cylinder to form a discharge channel. During operation, the lower belt captures the residual film discharged from the upstream collection device and conveys it toward the rear baling belt. After contacting the lower belt, the residual film is lifted and then falls back onto the accumulated film layer, forming an initial core through a winding process. As material continues to be supplied, the core grows progressively into a compact residual film bale. The formed bale is finally discharged from the rear of the device under the combined action of gravity and belt motion.

Baling Mechanism Design

The baling mechanism mainly consists of a lower baling mechanism and a rear baling mechanism. The lower baling mechanism includes a lower baling belt, a front drive roller, a rear drive roller, and support rollers. The rear baling mechanism consists of a rear baling belt, an upper drive roller, a lower drive roller, and support rollers. The two baling mechanisms are arranged symmetrically in a V-shaped configuration. Based on theoretical analysis and considering potential interference with the residual film recovery machine, the optimal angle between the two mechanisms was determined to be 70°.

The V-shaped space forms the baling chamber of the device, in which the residual plastic film is effectively compressed to form a residual film bale. To facilitate field operation and transportation, and to ensure that the bales can be discharged in a single operation, positioning blocks are installed on both sides of the belts to prevent lateral deviation caused by uneven tension during the baling process.

Due to the complex spatial structure of the baling chamber and the difficulty of precise analytical calculation, an estimation method based on the bale diameter is proposed to determine the appropriate size of the baling chamber. The calculation method is given as follows:

$$m = \rho \frac{\pi d^2}{4} l > \lambda LWX \tag{1}$$

In the formula, *m* represents the mass of a single residual film bale (kilograms), *ρ* is the density of the bale at discharge (kg/m^3), *d* is the diameter of the bale (m), *l* is the length of the bale (m), *L* is the maximum length of the field working row (m), *W* is the working width of the front-end residual film recovery machine (m), *X* is the mass of residual film per unit area (kg/m^2) and *λ* is the impurity coefficient of the bale.

The derivation of Equation (1) is based on the mass-volume equivalence principle. The mass of a single residual film bale (m) can be expressed as the product of the bale volume (V) and the mixture density (ρ) at the moment of discharge. Assuming that the bale is approximately cylindrical, with diameter (d) and length (l), its volume can be expressed as: $V = \frac{\pi d^2}{4} l$. Meanwhile, the total mass of residual film collected during a single operation can be expressed as the product of the working width (W), operation row length (L), residual film mass per unit area (X), and impurity coefficient (λ). By equating the two expressions and solving for (d) Equation (1) can be obtained.

To determine the impurity content of residual film per unit area in the experimental field, the following method was adopted. Random sampling was conducted in the test field, and five operation rows were selected. For each row, a standard sampling area of 8 m × 2.1 m was defined. The sampling process is illustrated in Fig. 2.

After the residual film within the sampling area was collected into the collection box using the residual film recovery machine, the data were analyzed. The corresponding measurement results are presented in Table 1.

Fig. 2 - Sampling and measurement of residual film during mechanical recovery

(1) Experimental field *(2) Residual film collection by the machine*

Table 1

Residual film mass in the experimental field

No.	Residual film mass / g	Residual film mass per unit area / kg/m ²
1	180.63	11.15×10-3
2	178.55	11.02×10-3
3	181.32	11.19×10-3
4	177.48	10.95×10-3
5	181.29	11.19×10-3
Average value	**179.85**	**11.10×10-3**

According to Table 1, the residual film mass per unit area (*X*) was taken as 9.46×10-3kg/m². Considering that the working width (*W*) of the residual film recovery machine is 2.1 m, the operating width of the proposed device was designed to match that of the 11CM-2100 residual film recovery machine; therefore, *W* was set to 2.1 m. The maximum measured operation row length (*L*) in the test field was 1000 m. The density of the residual film bale (ρ) was taken as 122.7 kg/m³ based on test results obtained from a roll-type residual film baling machine.

Eight groups of samples were randomly collected from the residual film mixture recovered by the machine. The analysis showed that the average volume ratio of residual film to impurities was 2.18:1.

Considering regional and crop-dependent variations in impurity content, and to ensure a sufficient design margin, the impurity coefficient (λ) was finally set to 2. Substituting these values into Equation (1) yields a minimum bale diameter of $d \geq 0.45$m. Taking into account the structural dimensions of the 11CM-2100 residual film recovery machine and avoiding interference with the baling device, a diameter of $d = 0.5\text{m}$ was selected as the design parameter. According to Equation (1), the corresponding bale mass (*m*) was calculated to be 57.33 kg. The designed residual film baling system is suitable for both manual handling and mechanized operation and meets ergonomic requirements.

Discrete element modelling of residual film

The residual film was modeled in Rocky DEM using the “flexible membrane” contact model, which allows for large deformation and bending behavior. Each film element was represented by a triangular mesh with assigned elastic properties: Young’s modulus of 0.2 GPa, Poisson’s ratio of 0.4, and a thickness of 0.05 mm. The contact interaction between film elements and the baling belts was defined using a linear spring-dashpot model, with a coefficient of restitution of 0.45, a static friction coefficient of 0.6, and a rolling friction coefficient of 0.15. These parameters were calibrated by comparing the simulated film stacking behavior with results from physical drop tests. The calibration process involved adjusting the friction coefficients until the simulated angle of repose matched the experimentally measured value of 38° for field-collected residual film samples. The simulation time step was set to 20% of the Rayleigh time step, and the total simulation time corresponded to 15 s of real operating conditions.

Establishment of the three-stage baling device model

During the simulation, observation of the dynamic behavior of the residual film revealed a stochastic scattering phenomenon, as shown in Fig. 3.

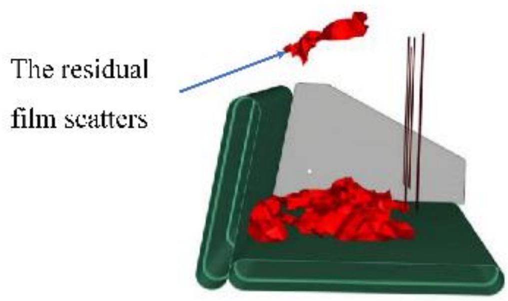

Fig. 3 - Residual film scattering phenomenon

When the residual film comes into contact with the rear baling belt, its relatively rough surface produces a hooking effect, leading to a sudden increase in frictional resistance. As a result, the residual film tends to scatter along the direction of belt motion. In actual operation, scattered film is prone to entanglement with transmission components or accumulation in structural gaps, which reduces operational efficiency and may cause blockage or mechanical failure. To address this issue, a third (upper) baling belt was introduced above the original lower and rear belts, forming a three-stage constraint system. This configuration significantly improves control over the motion trajectory of the residual film and effectively suppresses scattering

The upper belt serves two main functions. First, it intercepts residual film that deviates from the intended trajectory and redirects its motion through frictional interaction. Second, during bale formation, it works in coordination with the lower and rear belts to apply multi-directional compressive forces, resulting in improved compaction uniformity, higher bale density, and enhanced forming stability. The optimized three-stage structure is shown in Fig. 4.

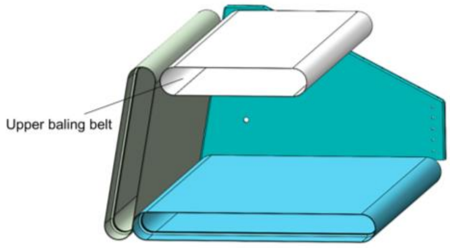

Fig. 4 - Three-stage residual film baling device

To investigate the influence of installation parameters on the baling performance, the installation inclination angle of the baling belt, the inclination angle of the baling chamber, and the belt linear speed were selected as experimental factors. The bale-forming rate and bale density were used as evaluation indicators, and single-factor experiments were conducted on the three-stage baling device.

The effect of the installation inclination angle on the device performance is shown in Fig. 5.

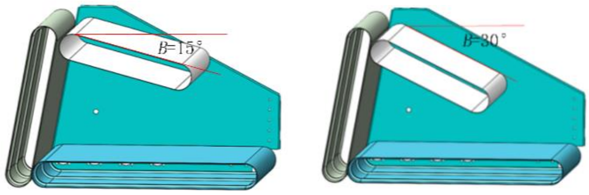

Fig. 5 - Installation inclination angle of the upper baling belt

The baling belt was selected as a rough-surface belt. The inclination angle of the baling chamber was set to 0°, the belt linear speed was fixed at 1.5 m/s, and the installation inclination angle of the upper belt was varied at 0°, 5°, 10°, 15°, 20°, 25°, and 30°. Each experiment was repeated five times, and the average values were used for analysis. The results are presented in Fig. 6.

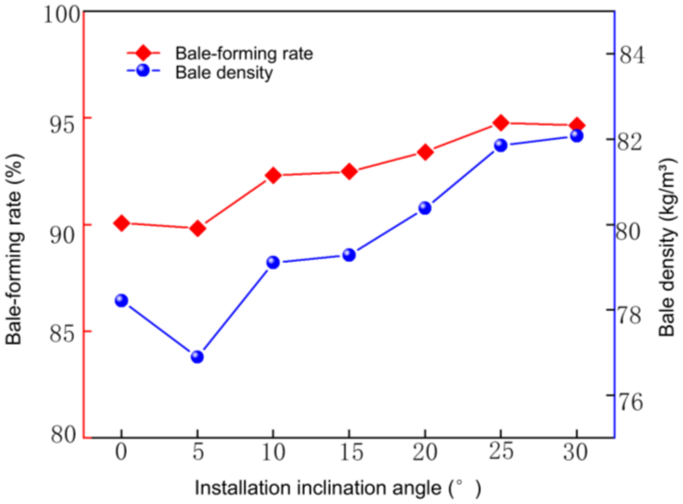

Fig. 6 - Effect of installation inclination angle on baling performance

It can be seen from Fig. 6 that the installation inclination angle of the upper baling belt has a significant influence on the forming quality of the residual film bales. As the inclination angle increases, both the bale-forming rate and bale density show an increasing trend, reaching optimal values at 30°. This behavior can be attributed to the fact that a larger inclination angle enhances the wrapping and normal constraint effects of the belt on the residual film. As a result, scattering during the compaction process is effectively suppressed, and the motion trajectory of the film becomes more stable, leading to improved bale formation and higher density.

A single-factor experiment was further conducted to investigate the effect of belt linear speed on the performance of the three-stage baling device. The installation inclination angle was fixed at 30°, and the inclination angle of the baling chamber was set to 0°. The belt linear speed was varied at 0.5 m/s, 1.0 m/s, 1.5 m/s, 2.0 m/s, and 2.5 m/s. Each experiment was repeated five times, and the average values were used for analysis. The results are shown in Fig. 7.

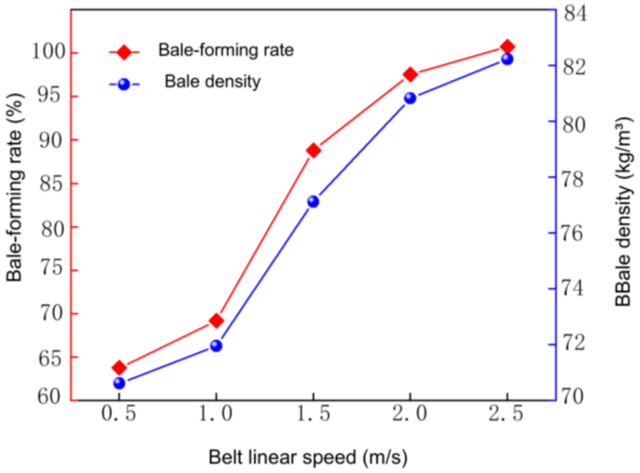

Fig. 7 - Effect of belt linear speed on baling performance

As shown in Fig. 7, compared with the conventional two-stage structure, the three-stage device exhibits clear advantages in terms of bale-forming rate and bale density. As the belt linear speed increases, both indicators show a continuous upward trend, reaching optimal values at 2.5 m/s. This behavior can be explained by the enhanced compaction effect provided by the third-stage belt. When the volume of the residual film bale reaches a certain level, the upper belt applies additional compressive force. By increasing the normal pressure and contact area, the overall frictional interaction and constraint on the residual film are significantly enhanced, resulting in improved bale integrity and higher density.

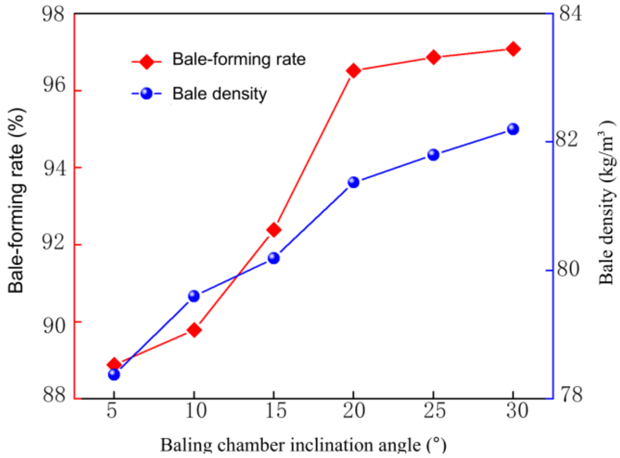

Fig. 8 - Effect of baling chamber inclination angle on baling performance

A single-factor experiment was conducted to investigate the effect of the baling chamber inclination angle on the performance of the three-stage baling device. The installation inclination angle of the upper belt was fixed at 30°, and the belt linear speed was set to 1.5 m/s. The results are presented in Fig. 8. As the baling chamber inclination angle increases, both the bale-forming rate and bale density exhibit an increasing trend. This is because a larger inclination angle enhances the spatial constraint during the compaction process. In combination with the three-stage belt system, a multi-directional constraint is formed, which effectively controls the motion trajectory of the residual film, improves material aggregation, enhances compaction, and reduces scattering.

RESULTS

Simulation performance test of three-stage baling device

To investigate the performance variation of the three-stage residual film baling device under multi-factor conditions, and to identify the key variables affecting bale density and bale-forming rate, an orthogonal experimental design was adopted to determine the optimal operating parameter combination. The belt linear speed, the installation inclination angle of the upper belt, and the inclination angle of the baling chamber were selected as experimental factors. The corresponding factor levels are presented in Table 2.

Table 2

Factor levels of the three-stage baling device

Level	Baling chamber inclination angle A/°	Upper belt inclination angle B/°	Belt linear speed C/m·s^{-1}
-1	20	20	2.1
0	25	25	2.3
1	30	30	2.5

Analysis of experimental data

A simulation experiment was designed using the Box–Behnken method. A total of 17 experimental runs were conducted, including five replications at the center point. The experiments were designed to investigate the interaction effects between the bale-forming rate, bale density, and three key factors.

Regression model for bale-forming rate

Analysis of variance (ANOVA) and significance tests of the regression coefficients were performed for the regression model of the residual film bale-forming rate (Y_1). The regression equation for Y_1 is given as follows:

$$\hat{Y}_1 = 97.38 + 0.635A + 0.8345B + 0.6162C + 0.0075AB - 0.1042AC + 0.11BC + 0.3117A^2 - 0.1008B^2 - 1.52C^2 \quad (2)$$

Taking the bale-forming rate as the response variable, the regression model established for the baling chamber inclination angle (*A*), the upper belt inclination angle (*B*), and the belt linear speed (*C*) was found to be highly significant (F = 402.8). The linear terms (*A*, *B*, *C*), interaction terms (*AC*, *BC*), and quadratic terms (A^2, B^2, C^2) were all statistically significant. The lack-of-fit term was not significant (F = 2.0, p = 0.2565), indicating good model adequacy. The coefficient of determination was R^2 = 0.9981, with an adjusted R^2 of 0.9956 and a predicted R^2 of 0.9803, demonstrating excellent model fit and strong predictive capability.

Based on response surface methodology (RSM), the experimental data were analyzed to investigate the interaction effects between the bale-forming rate and its key influencing factors, as shown in Fig. 9.

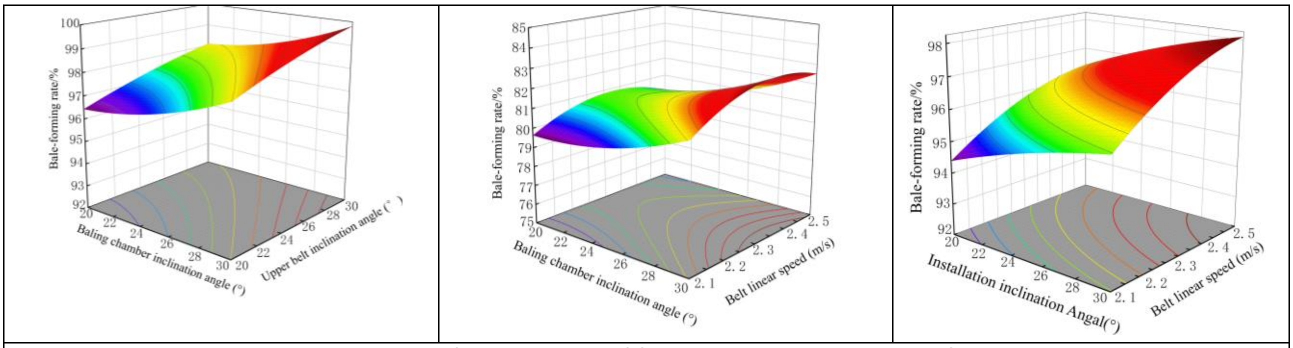

Fig. 9 - Response surface analysis of factor interactions on bale-forming rate

(a) Interaction between baling chamber inclination angle and upper belt inclination angle | *(b) Interaction between baling chamber inclination angle and belt linear speed* | *(c) Interaction between upper belt inclination angle and belt linear speed*

Figure 9(a) shows that the bale-forming rate increases with the increase in the upper belt inclination angle, and its influence is more significant than that of the baling chamber inclination angle. This trend can be explained by the change in force components acting on the residual film. As the inclination angle increases, the normal force component exerted by the upper belt becomes more effective in constraining the film, while the tangential (conveying) component also increases, improving both compaction and motion control. Consequently, the probability of film scattering is reduced.

Figure 9(b) indicates that, under the interaction between belt linear speed and baling chamber inclination angle, the bale-forming rate initially increases and then decreases with increasing belt speed, reaching a peak value (approximately 81.5%) at around 2.3 m/s. The influence of belt linear speed is more pronounced than that of the baling chamber inclination angle.

Figure 9(c) shows that the response surface for the interaction between belt linear speed and upper belt inclination angle is convex, indicating the presence of an optimal parameter region. The effect of the upper belt inclination angle on the bale-forming rate is more significant than that of belt linear speed.

The variation in bale density follows a similar trend. The maximum density is also achieved at approximately 2.3 m/s, as optimal compaction requires both sufficient compressive force and adequate residence time for interlayer bonding of the residual film. At excessively high belt speeds, the residence time in the compression zone is reduced, limiting effective compaction.

According to the response surface analysis, the order of influence of each factor on the bale-forming rate is: upper belt inclination angle > baling chamber inclination angle > belt linear speed

Regression model for bale density

The regression model for residual film bale density (Y_2) was analyzed using ANOVA and significance tests of the regression coefficients. The regression equation for Y_2 is given as follows:

$$\hat{Y}_2 = 81.35 + 1.03A + 1.21B + 0.4217C - 0.0075AB - 0.055AC + 0.11BC + 0.5051A^2 - 0.3983B^2 - 0.9424C^2 \quad (3)$$

The developed regression model for bale density was found to be highly significant (F = 875.1). The linear terms (A, B, C), interaction terms (AC, BC), and quadratic terms (A^2, B^2, C^2) were all statistically significant. The lack-of-fit term was not significant (F = 4.73, p = 0.0838), indicating good model adequacy. The coefficient of determination was R^2 = 0.9988, with an adjusted R^2 of 0.9973 and a predicted R^2 of 0.9849, demonstrating excellent agreement between the model and experimental data, as well as strong predictive capability.

Based on response surface methodology, the interaction effects of each factor on bale density were analyzed, and the corresponding response surface plots are shown in Fig. 10.

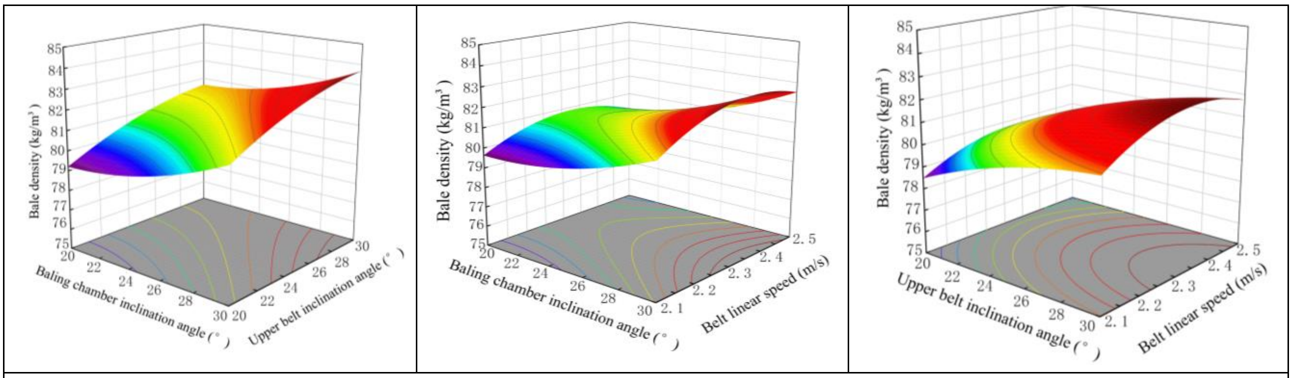

Fig. 10 - Response surface analysis of factor interactions on bale density

(a) Interaction between baling chamber inclination angle and upper belt inclination angle	*(b) Interaction between baling chamber inclination angle and belt linear speed*	*(c) Interaction between upper belt inclination angle and belt linear speed*

Figure 10(a) shows that bale density increases with increasing upper belt inclination angle, and its influence is more significant than that of the baling chamber inclination angle. Figure 10(b) indicates that, under the interaction between belt linear speed and baling chamber inclination angle, bale density initially increases and then decreases with increasing belt speed, reaching a peak value of approximately 81.2 kg/m³ at around 2.3 m/s. The interaction between these two factors is significant. Figure 10(c) shows that, under the interaction between belt linear speed and upper belt inclination angle, the influence of the upper belt inclination angle on bale density is more pronounced than that of belt linear speed.

To determine the optimal operating parameters, the regression models were optimized using Design-Expert software. The constraints were set as follows: baling chamber inclination angle of 25°–30°, upper belt inclination angle of 20°–30°, and belt linear speed of 2.1–2.5 m/s. The optimization results indicate that the maximum bale density (83.75 kg/m³) is achieved at a baling chamber inclination angle of 29.92°, an upper belt inclination angle of 29.64°, and a belt linear speed of 2.3 m/s. Meanwhile, the maximum bale-forming rate (99.13%) is obtained at a baling chamber inclination angle of 29.96°, an upper belt inclination angle of 30.11°, and a belt linear speed of 2.33 m/s.

Considering manufacturing feasibility and operational convenience, the final selected parameter combination was a baling chamber inclination angle of 30°, an upper belt inclination angle of 30°, and a belt linear speed of 2.3 m/s.

Performance tests of the residual film baling device were then conducted. Based on the average of 10 trials, the results (Table 6) show that the measured bale density was 91.4 kg/m³, and the bale-forming rate reached 100%. The experimental results are in good agreement with the simulation predictions, demonstrating the feasibility and accuracy of the proposed simulation model. The operational performance of the machine is shown in Fig. 11.

Fig. 11 - Experimental setup for performance testing of the residual film baling device

Table 3

Experimental results of bale density and bale-forming rate

Test Number	**1**	**2**	**3**	**4**	**5**
bale-forming rate Y_1/(%)	91.3	92.5	90.8	89.4	93.7
Test Number	6	7	8	9	10
bale-forming rate Y_1/(%)	88.5	91.1	90.2	93.8	92.7
Average value	91.4				
Test Number	1	2	3	4	5
bale density Y_2(kg·m^{-3})	100	100	100	100	100
Test Number	6	7	8	9	10
bale density Y_2%(kg·m^{-3})	100	100	100	100	100
Average value	100				

CONCLUSIONS

(1) The proposed three-stage baling structure significantly improved baling performance. By introducing an upper baling belt to the conventional two-stage configuration, a three-dimensional constraint system was formed. This effectively suppressed residual film scattering and enhanced bale compactness. Both the bale-forming rate and bale density were significantly improved compared with the traditional two-stage structure.

(2) The optimal combination of operating parameters was determined using response surface methodology. For the three-stage baling device, the optimal conditions were a baling chamber inclination angle of 30°, an upper belt inclination angle of 30°, a belt linear speed of 2.3 m/s, and the use of a rough-surface belt. Under these conditions, the maximum bale-forming rate reached 99.13%, and the bale density reached 83.75 kg/m³, indicating optimal operational performance.

(3) Field tests verified the reliability of the simulation results and the practicality of the device. Under the optimized parameters, the measured average bale density was 91.4 kg/m³. The experimental results were in good agreement with the simulation predictions, demonstrating the high predictive accuracy of the developed model. The device operated stably and reliably, meeting the requirements for residual film recovery in farmland conditions.

(4) This study provides a feasible technical solution for efficient residual film recovery and pollution control. Through structural innovation and systematic parameter optimization, the device achieved high bale-forming rates and high-density compaction. This contributes to improved recovery efficiency and reduced post-processing costs, with positive implications for mitigating residual film pollution in agricultural fields.

Although the DEM model captures the main flexible behavior of residual film, it simplifies the material as a homogeneous elastic shell and does not account for tear propagation or variable impurity adhesion. The model parameters were calibrated under dry, low-impurity conditions; their applicability to wet or high-impurity environments requires further validation. In addition, the scalability of the optimal parameters to different crop types (e.g., maize vs. cotton) and field conditions has not been systematically investigated. The long-term durability of the three-stage belt system (e.g., belt wear and tension stability) will be evaluated in future multi-season field trials.

ACKNOWLEDGEMENT

Fund Project: Key Research Project of Basic Scientific Research of Liaoning Provincial Department of Education in 2022, Project Number (LJKZZ20220158)

Project of Liaoning Vocational College of Agriculture: Design of Farmland Film Recovery Device (LnzkA202405).

REFERENCES

[1] Anderson, G., Smith, L., Roberts, K. (2021). Plastic waste management in agriculture: Policy implications. *Environmental Policy and Governance*, 31(2):101-109.

[2] Chen, L., Wang, F., Xu, P. (2020). Efficiency of agricultural film recovery machines. *Applied Engineering in Agriculture*, 36(5):745-751.

[3] Choi, J., Park, S., Lee, H. (2021). Engagement strategies for effective film recovery implementation. *Sustainable Development*, 29(6):660-670.

[4] Deng, Y., Liu, J., He, W. (2022). Assessing farmer attitudes towards plastic film recovery. *Agricultural Systems*, 197:103-110.

[5] Gao, J., Liu, Y., Zhao, X. (2022). Enhancing recovery efficiency in agricultural practices. *Bioresource Technology Reports*, 10:123-132.

[6] Huang, X., Zhang, D., Wei, J. (2020). Circular economy in agriculture: A review of plastic recovery systems. *Sustainable Production and Consumption*, 24:33-42.

[7] Kim, S., Lee, D., Park, J. (2021). Recycling potential of agricultural films: Challenges and opportunities. *Waste Management*, 120:54-62.

[8] Li, J., Zhang, H., Wang, L. (2021). Environmental impacts of agricultural plastic waste. *Waste Management*, 119:35-45.

[9] Liu, H., Zhang, H. (2019). Assessment of agricultural plastic waste management. *Resources, Conservation and Recycling*, 148:55-62.

[10] Liu, L., Zhang, D., Qiu, F. (2022). The importance of education in plastic waste management. *International Journal of Agricultural Sustainability*, 20(3):227-237.

[11] Mao, Q., Liu, T., Chen, Y. (2022). The role of plastic recovery in sustainable agriculture. *Journal of Environmental Management*, 303:113-120.

[12] Potyondy, D.O., Cundall, P.A. (2004). A bonded-particle model for rock. International Journal of Rock Mechanics and Mining Sciences, 41(8):1329-1364.

[13] Roberts, K., Brown, S., Wang, T. (2022). The circular economy in agricultural management. *Journal of Sustainable Agriculture*, 35(4):789-800.

[14] Roessler, T., Katterfeld, A. (2018). DEM parameter calibration of cohesive bulk materials using a simple angle of repose test. Particulate Science and Technology, 36(8):982-992.

[15] Smith, R., Brown, A., Taylor, M. (2019). Economic impacts of film recycling on farmers. *Agricultural Economics*, 50(1):110-120.

[16] Tan, C., Gao, H., Wu, F. (2022). Future directions in agricultural film recovery research. *Journal of Cleaner Production*, 350:131-145.

[17] Torres, A., Kim, S., Garcia, R. (2022). Cost-benefit analysis of film recovery systems. *Journal of Cleaner Production*, 345:131-140.

[18] Wang, T., Liu, P., Sun, Z. (2021). Innovations in plastic film recovery technologies. *Journal of Agricultural Engineering*, 8(3):123-133.

[19] Xie, F., Liu, Z., Cheng, B. (2020). Sustainable technologies for agricultural waste management. *Journal of Environmental Science and Health*, 55(12):1450-1460.

[20] Xu, P., Zhang, J., Li, Q. (2023). Labor savings through automated film recovery techniques. *Frontiers in Sustainable Food Systems*, 7:220-230.

[21] Yuan, T., Zhang, L., Chen, H. (2023). Overcoming barriers to film recovery technology adoption. *Renewable Agriculture and Food Systems*, 38(1):56-68. Zhang, Y., Chen, L., Li, C. (2020). Microplastic pollution in agricultural soils: A review. *Agronomy for Sustainable Development*, 40(2):15.